Nanoscale

Accepted Manuscript

This article can be cited before page numbers have been issued, to do this please use: M. Raissi, M. T. Sajjad, Y. Pellegrin, T. roland, S. Jobic, M. Boujtita, A. Ruseckas, I. D. W. Samuel and F. Odobel, *Nanoscale*, 2017, DOI: 10.1039/C7NR03698A.

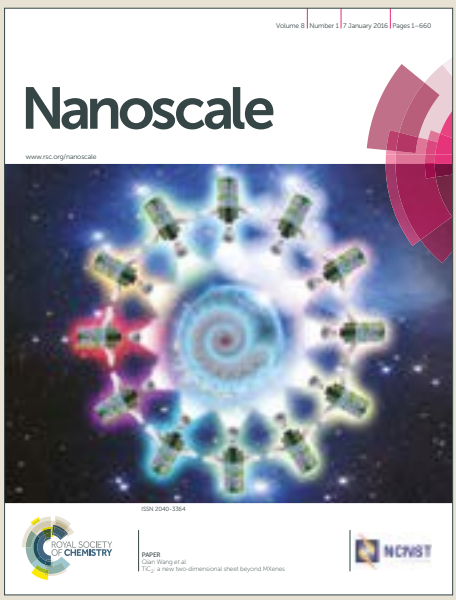

View Article Online
DOI: 10.1039/C7NR03698A

Size dependence of efficiency of PbS quantum dots in NiO-based dye sensitised solar cells and mechanistic charge transfer investigation

Mahfoudh Raissi,[a†] Muhammad T. Sajjad,[b†] Yann Pellegrin,[a] Thomas Jean Roland,[b] Stéphane Jobic,[c] Mohammed Boujtita,[a] Arvydas Ruseckas,[b] Ifor D. W. Samuel,[*b] Fabrice Odobel*[a]

†these two persons equally participate to the work

[a]*CEISAM, Chimie Et Interdisciplinarité, Synthèse, Analyse, Modélisation, CNRS, UMR CNRS 6230, UFR des Sciences et des Techniques ; 2, rue de la Houssinière - BP 92208; 44322 NANTES Cedex 3 (France)*
E-mail: Fabrice.Odobel@univ-nantes.fr
[b]*Organic Semiconductor Centre, SUPA, School of Physics and Astronomy, University of St Andrews, North Haugh, St Andrews, KY169SS, United Kingdom.*
E-mail: idws@st-andrews.ac.uk
[c]*Institut des Matériaux Jean Rouxel, Université de Nantes, CNRS, 2, rue de la Houssinière, BP 32229, 44322 Nantes cedex 03, France*

Abstract

Quantum dots (QDs) are very attractive materials for solar cells due to their high absorption coefficients, size dependence and easy tunability of their optical and electronic properties due to quantum confinement. Particularly interesting are PbS QDs owing to their broad spectral absorption until the long wavelengths, their easy processability and low cost. Here, we used control of the PbS QDs size to understand charge transfer processes at the interfaces of NiO semiconductor and explain the optimal QDs size in photovoltaic devices. Towards this goal, we have synthesized a series of PbS QDs with different diameters (2.8 nm to 4 nm) and investigated charge transfer dynamics by time resolved spectroscopy and their ability to act as sensitizers in nanocrystalline NiO based solar cells using the cobalt tris(4,4'-diterbutyl-2,2'-bipyridine) complex as redox mediator. We found that PbS QDs with average diameter of 3.0 nm are optimal size in terms of efficient charge transfers and light harvesting efficiency for photovoltaic performances. Our study showed that hole injection from PbS QDs to NiO valence band (VB) is an efficient process even with low injection driving force (0.3 eV) and occurs in 6−10 ns. Furthermore we found that the direct electrolyte reduction (photoinduced electron transfer to the cobalt redox mediator) also occurs in parallel to the hole injection with rate

View Article Online
DOI: 10.1039/C7NR03698A

constant of similar magnitude (10-20 ns). In spite of its large driving force, the rate constant of the oxidative quenching of PbS by Co(III) diminishes more steeply than hole injection on NiO when the diameter of PbS increases. This is understood as the consequence of increasing the trap states that limit electron shift. We believe that our detailed findings will advance the future design of QD sensitized photocathodes.

Introduction

Design of novel sensitized NiO photocathodes with wide visible light absorption and good stability is of great significance for tandem dye sensitized solar cells[1] and for photoelectrochemical devices for hydrogen evolution[2] or carbon dioxide reduction.[3] Indeed, the development of efficient and stable photocathodes that can successfully serve the above practical applications is still a great challenge. Quantum dots (QDs) are very attractive light collectors to sensitize wide bandgap semiconductors such as TiO_2[4] (n-type semiconductor) or NiO (p-type semiconductor) as there are several successful demonstrations of their efficiencies in solar cells and in photoelectrocatalytic devices. For example, quantum dot sensitized solar cells (QDSSCs) using NiO as the semiconductor have been reported with nanocrystals of CdS,[5] CdSe,[6] Cu_2S,[7] $CdTeO_3$[8] and $CuInS_2$,[9] and more recently we have reported the potential of PbS[10] QDs notably to exploit the near infrared (IR) region of solar spectrum, which contains about 50% of the solar spectrum photons. Metal chalcogenides were also successfully implemented in NiO based photoelectrocatalytic devices for solar hydrogen evolution.[11] These successes clearly illustrate the great potential of quantum dots to act as efficient and stable sensitizers for p-type semiconductors such as NiO. As mentioned above, lead sulfide (PbS) is an attractive material owing to its low bandgap, which makes it very valuable for harvesting low energy photons of the visible spectrum and the near infrared (NIR). The good photovoltaic performance of p-QDSSC with PbS nanocrystals reported earlier[10, 12] prompted us to investigate deeper the potential of this system and the operation mechanism of the solar cells. Herein, we have focused on how the photovoltaic performance is determined by the PbS size and investigated in detail the operation principle of p-QDSSC with time resolved photoluminescence spectroscopy. In this paper, we demonstrate optimization of QDSSCs by investigating the size dependence of PbS nanocrystal on the photovoltaic performances. We have identified that hole injection from PbS QD to NiO valence band (VB) occurs in 6−10 ns, while the photoinduced electron transfer to the cobalt redox mediator is on the timescale of 10-20 ns. Accordingly, both processes (photovoltaic and photogalvanic) occur in parallel. Moreover, an important finding of this study is the relatively high hole injection efficiency in NiO in spite of the low driving force (around -0.3 eV).

View Article Online
DOI: 10.1039/C7NR03698A

Results

Preparation of the PbS nanocrystals

The PbS quantum dots used in this study were all synthesized according to the so-called hot injection method using a procedure adapted from Hines and Scholes.[13] It is based on the reaction of a solution of lead oleate ($Pb(OA)_2$) with bis(trimethylsilyl) sulfide $(TMS)_2S$ as a source of sulfide anion:

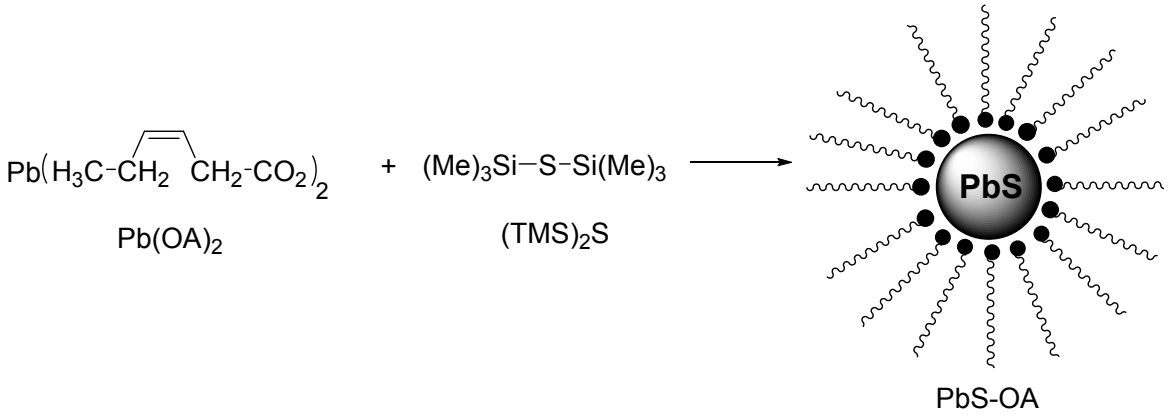

The control of the reaction temperature (between 90°C and 130°C) and of the concentration of oleic acid (OA) of the initial lead oleate solution enables the quantum dot size to be precisely tuned from 2.8 nm to 3.4 nm (see experimental part for details). High temperatures and large concentrations of OA promote the formation of large sizes QDs because as the high concentration of OA slows down the kinetic of the nucleation step.[13b] The quantum dots were purified by three cycles of precipitation into acetone and redispersed in n-octane. The resulting QDs were capped with a monolayer of oleate ligands, and it is known that they contain a significant amount of traps owing to the presence of surface dangling bonds. [4f, 14] As reported before, these traps were passivated with iodide ligands upon treatment of the PbS quantum dots with a solution of tetrabutylammonium iodide (TBAI).[14-15] Indeed, the iodide anion is a sufficiently small ligand to infiltrate inside of the OA shell and to chelate the surface free lead atom. The passivation of these intragap states is crucial to achieve high photovoltaic performance, because they quench the exciton, reducing its lifetime and consequently also reducing the quantum yield for charge transfer. Finally, the film was treated with a solution of cetyl trimethyl ammonium bromide (CTAB) to substitute further some more OA ligands by halides. We have observed that this treatment is crucial to diminish the thickness of the insulating shell of OA and to induce a closer distance between PbS and NiO surface.[10] It also increases the density of QD grafted onto the NiO surface in the second cycle of loading, most probably by reducing the footprint of the QD. The QD loading is repeated a second time to maximize the amount of PbS grafted on the NiO surface.

View Article Online
DOI: 10.1039/C7NR03698A

The QD diameter was determined from two independent methods and they were both fully consistent. First, the optical bandgap (Eg) deduced from the absorption spectrum in solution was used to calculate the nanocrystal diameter (d) from the empirical equation reported by Iwan and Moreels[16]:

$$Eg = 0.41 + (0.0252d^2 + 0.283d)^{-1} \qquad (1)$$

The optical bandgap (Eg) was calculated from the wavelength on the excitonic peak (λ) according to the equation:

$$Eg(eV) = 1240/\lambda(nm) \qquad (2)$$

Table 1. Absorption and emission characteristics and bandgap of the prepared PbS QDs.

entry	d[a] (nm)	T°C[b]	λ_{abs}[c] (nm)	ε_{abs}[d] ($M^{-1}cm^{-1}$)	λ_{em}[e] (nm)	Eg op (eV)	E_{BV}(PbS) (V/ECS)	E_{BC}(PbS) (V/ECS)
1	2.8	90	884	42800	969	1.40	0.62±0.06	-0.78±0.06
2	2.9	100	905	46410	990	1.37	0.55±0.06	-0.80±0.06
3	3.0	110	925	50210	1008	1.34	0.48±0.06	-0.70±0.06
4	3.2	120	995	58320	1036	1.25	0.52±0.06	-0.69±0.06
5	3.4	130	1048	67130	1081	1.18	0.52±0.06	-0.67±0.06

[a]determined from Iwan and Moreels equation 1; [b]reaction temperature; [c]excitonic peak recorded in toluene; [d]determined from the equation 3; [e]emission wavelength recorded in toluene,

High resolution transmission electron microscopy (HRTEM) is the second technique that was used to determine the size of the PbS nanocrystals (Figure 1). The TEM pictures show that all the prepared QDs have spherical shape and a quite narrow size distribution. The diameters measured on the HRTEM pictures agree, within experimental error, very well with the value extracted from the optical bandgap (Table 1 and Table S1).

View Article Online
DOI: 10.1039/C7NR03698A

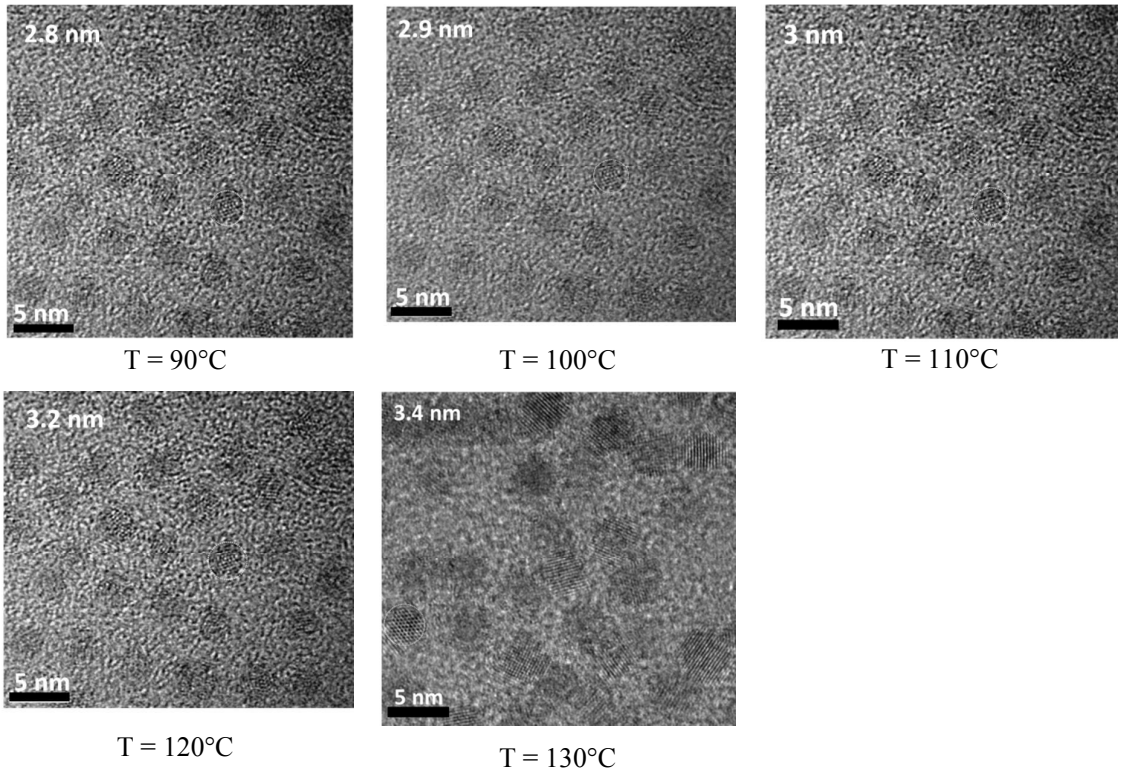

Figure 1. HRTEM pictures of the PbS-OA nanocrystals prepared in this study as a function of the reaction temperature.

Electronic absorption and steady state emission spectra

The electronic properties of the quantum dots capped with OA only (PbS-OA) were first examined with the measurements of their electronic absorption and emission spectra recorded in toluene solution (Figure 2). The extinction coefficients were calculated from equation (3) developed by Ozin and co-workers[17]:

$$\varepsilon(PbS) = 19600r^{2.32} \qquad (3)$$

where r is the radius of the PbS nanocrystal. The maximum absorption wavelengths, the extinction coefficients and emission wavelengths are collected in Table 1.

View Article Online
DOI: 10.1039/C7NR03698A

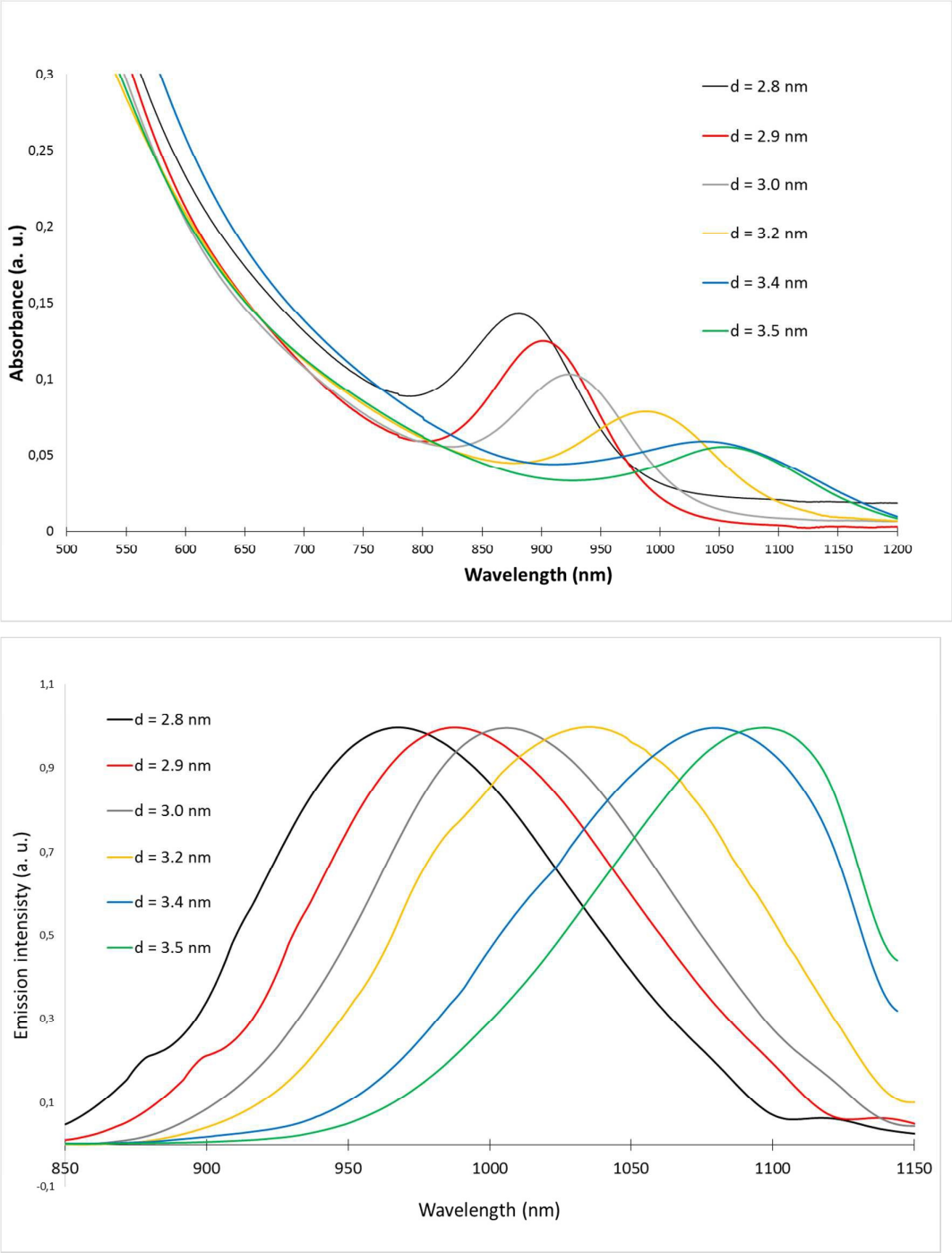

Figure 2. Absorption (upper panel) and normalized emission (lower panel) spectra of the PbS-OA quantum dots recorded in toluene solution. The samples were excited at 700 nm for all emission spectra.

The absorption spectra of the quantum dots treated with TBAI (PbS-TBAI) are slightly altered, with a bathochromic shift of about 5 nm on the excitonic peak (see supplementary information Figure S1 and

View Article Online
DOI: 10.1039/C7NR03698A

Table S2). This small change does not significantly impact the bandgap and most probably does not affect much the conduction and valence band positions.

Determination of the position of the PbS valence band potential and calculations of the charge transfer Gibbs free energies for the charge transfer reactions

The determination of the position of the valence band (VB) and conduction band (CB) potentials of the PbS QDs is important for calculating the Gibbs free energies of the various charge transfer processes taking place between the PbS nanocrystal and NiO and with the redox mediator. The valence band potentials were determined by recording cyclic voltammetry of the PbS-OA QDs in acetonitrile with tetrabutylammonium hexafluorophosphate (Bu_4NPF_6) as supporting electrolyte with a conventional one compartment three electrode setup.[18] These experiments were attempted with PbS-TBAI but the wave of the iodide oxidation does not permit to observe that of PbS. However, owing to the slight variation of the bandgap between PbS-OA and PbS-TBAI (ΔEg = 0.03 eV at maximum), we can reasonably assume that the alteration of the position of the VB upon treatment with TBAI is really weak. A few drops of the colloidal solution of PbS QDs were deposited on the surface of the platinum working electrode and dried in the air before the cyclic voltammetry was recorded. Prominent and highly irreversible cathodic and anodic waves were observed on the voltammograms. The irreversibility of the electrochemical processes is usual for QDs immobilized on electrodes due to the detachment of the QDs from electrode surface upon oxidation or reduction. A typical voltammogram is given in Figure S2 in supplementary information. All potentials reported in this paper are referenced relative to saturated calomel electrode (SCE) and they are collected in Table 1.

The Gibbs free energy of the hole injection reaction into the valence band of NiO (ΔG_{inj}) is the energy associated with the oxidation of NiO and the reduction of PbS corresponding to the difference of the VB potentials of PbS and NiO:

$$\Delta G_{inj} = E_{VB}(PbS) - E_{VB}(NiO) \quad (4)$$

The numerical values of are gathered ΔG_{inj} in Table 2. Clearly as the diameter of the PbS nanocrystal increases the hole injection driving force steadily decreases until reaching a low value for d = 3.4 nm (ΔG_{inj} = -0.22 eV).

View Article Online
DOI: 10.1039/C7NR03698A

Table 2. Valence band (VB) and conduction band (CB) potentials of the prepared PbS-OA along with the hole injection and regeneration Gibbs free energies. All potentials are referenced relative to saturated calomel electrode (SCE).

entry	d[a] (nm)	ΔG_{inj}[a] (eV)	ΔG_{reg}[b] (eV)
1	2.8	-0.32±0.06	-0.87±0.06
2	2.9	-0.25±0.06	-0.89±0.06
3	3.0	-0.18±0.06	-0.79±0.06
4	3.2	-0.22±0.06	-0.78±0.06
5	3.4	-0.22±0.06	-0.76±0.06

[a]determined from the equation (4) with E_{VB}(NiO) 0.3 V vs SCE; [b]calculation from the equation (5) using $E(Co^{III/II})$= 0.09 V vs SCE.

The free energy of the regeneration reaction (ΔG_{reg}) taking place between the reduced quantum dot and the electrolyte is simply given by the difference of the redox potential of the $Co^{III/II}$ complex and the conduction band potential of PbS according to the equation:

$$\Delta G_{reg} = E_{CB}(PbS) - E(Co^{III/II}) \qquad (5)$$

The data are summarized in Table 2 and show that this reaction is very exergonic for all sizes of the QDs. Finally, it is also interesting to assess the Gibbs free energy for the reduction of the cobalt electrolyte (ΔG_{red}) from the photoexcited PbS quantum dot. This driving force can be approximatively similar to ΔG_{reg} because the one electron reduced QD and the exciton into the photoexcited PbS quantum dot can be considered to have the same reducing power. Again, the calculations indicate that the direct electron transfer from the photoexcited PbS quantum dot to the Co(III) complex in solution is a very thermodynamically favorable reaction.

Overall, the reduction of the Co(III) redox shuttle in the electrolyte either from the reduced QD or from the photoexcited QD are both very exergonic processes independently of the size of the PbS nanocrystal, while the hole injection reaction has a much lower driving force, which steeply decreases to very low values as the diameter of the QD increases.

View Article Online
DOI: 10.1039/C7NR03698A

Photophysical study

The different charge transfer steps potentially involved in the p-DSSCs are summarized in Scheme 1. The main objective of this photophysical study is to have an insight on the photovoltaic mechanism involved in this p-QDSSC *via* the determination of the rate constants of the charge transfer processes occurring in the system, that is the charge exchange between NiO and the PbS quantum dot (reaction 3) and between PbS and the electrolyte (reaction 4) occurring after light absorption by PbS QD (reaction 1). Indeed, the exact sequence of the electron transfer chain has never been investigated in quantum dot sensitized NiO semiconductor.

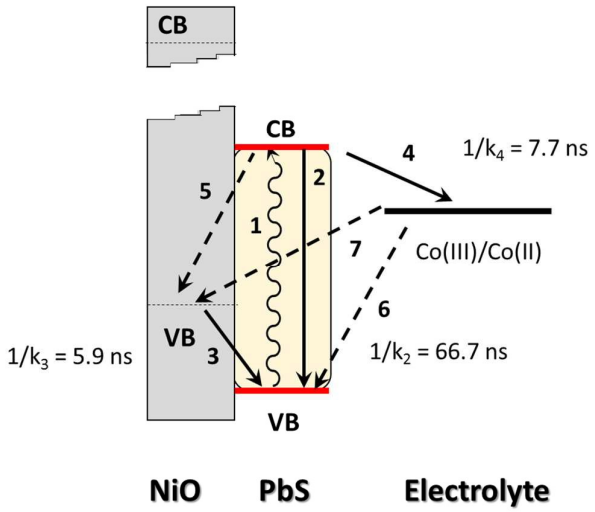

Scheme 1. Representation of the charge transfer reactions involved in the p-QDSSC. Dashed lines correspond to charge recombination reactions. The direction of the arrow indicates the movement of the electron. The rates indicated on the arrows correspond to those with PbS-TBAI with diameter = 3.0 nm.

Upon light excitation of PbS an exciton is created in the nanocrystal corresponding to the electron transfer from the VB to the CB (reaction 1). The exciton can decay following several pathways. First, radiative decay (reaction 2) or hole injection into NiO can take place (reaction 3). If the hole injection reaction occurs, then the electron residing on the CB of PbS can either recombine with hole in NiO (reaction 5) or can be shifted to the cobalt(III) complex in solution (reaction 4). Conversely, the photoexcited QD can first react with the electrolyte and reduce the cobalt(III) complex (reaction 4), then the hole in PbS can be either injected in NiO (reaction 3) or recombine with the cobalt(II) complex in solution (reaction 6). Another important recombination reaction found in NiO based p-DSSC is the interfacial charge recombination of the redox shuttle in the electrolyte with the injected holes in NiO (reaction 7).[19] The sequence of the charge transfer chain has most certainly an impact on

View Article Online
DOI: 10.1039/C7NR03698A

the photovoltaic performances of the solar cell. This prompted us to investigate the kinetics of the processes occurring from the photoexcited PbS.

Towards this goal, we have used PbS-TBAI nanocrystals with diameter 3.0 nm giving the optimal photovoltaic performances along with the diameter of 3.4 nm having a weaker PCE and an additional QD with 4.0 nm which was specially prepared for this study in order to confirm the trend of the photoluminescence measurements. The luminescence lifetime measurements were recorded in different environments by time resolved spectroscopy using excitation wavelength at 640 nm and photoluminescence was detected using a Hamamatsu infrared streak camera (C11293). First, the PbS QDs were grafted on mesoporous alumina films according to exactly the same procedure as that used for NiO photocathodes (see experimental part). The photoluminescence decay of PbS luminescence was monitored in presence of the electrolyte lacking the redox couple (propylene carbonate+ $LiClO_4$) to provide the reference lifetime of PbS emission without quencher (reaction 2 on Scheme 1) and then in the presence of the oxidized species of the redox shuttle (Co(III) and Co(II) complexes) to determine the rate constant of the photoinduced electron transfer to Co(III) (reaction 4 on Scheme 1), that is the oxidative quenching of the QDs. Alumina exhibits a VB and a CB located far apart from those of PbS, this guarantees the absence of any charge transfer reaction between all the QDs and this oxide. The lifetime measurements were also performed on the NiO films coated with PbS QDs. First, measurements were conducted in the absence of the cobalt complex in the electrolyte solution to determine the hole injection rate constant (reaction 3 on Scheme 1) and then in the presence of the Co(III) and Co(II) complexes to meet the exact conditions of the solar cells. The normalized photoluminescence decays of the PbS QD with diameter =3.0 nm are shown in Figure 3 (left panel) those of larger sizes are shown in Figure S3 in supplementary information.

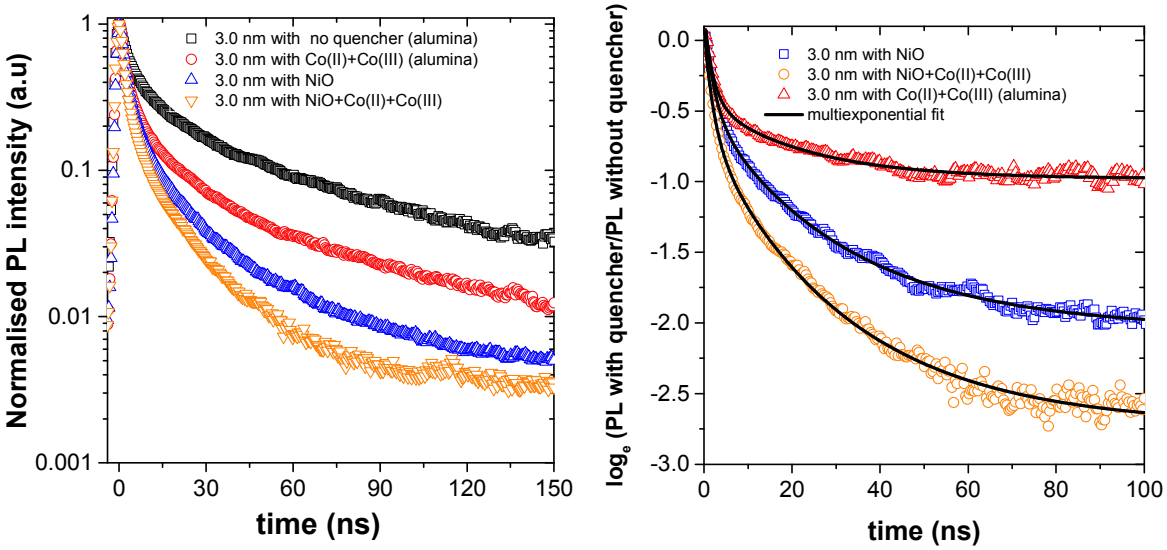

View Article Online
DOI: 10.1039/C7NR03698A

Figure 3. (left panel) Normalized photoluminescence decays of the PbS QDs (d=3.0 nm) recorded in different environments. (right panel) Ratio of photoluminescence kinetics of the 3.0 nm PbS QDs with quencher (electron/hole acceptor) to photoluminescence kinetics without quencher (i.e on alumina) The solid black lines are fits to PL decays

On alumina films without quencher, the emission decays are relatively long for smaller size PbS QDs and shorter for the larger size PbS (the emission decays of different size of PbS QDs on alumina are given in Figure S4 in supplementary information). Clearly, as the diameter of PbS increases the emission lifetime is shortened (Table 3). This can be interpreted as the consequences of energy gap law and the enhancement of the number of traps as the surface of nanocrystal increases. Moreover, for all sizes of QDs the emission decay is much longer on alumina films with neutral electrolyte than on films with electron/hole quencher (Co(III) or NiO). In presence of a quencher (Co(III) or NiO), the PbS emission lifetimes are greatly shortened relative to that of the reference and the decays are multiexponentials as is always observed on mesoporous semiconductor surfaces with NiO and TiO_2 films (Figure 3).[32] The reduced emission lifetimes both in the presence of Co(III) and on NiO confirms that the exciton in PbS can be quenched both reductively (by hole injection into NiO) and oxidatively (by photoinduced electron transfer to Co(III)) with high quantum yields. This result is particularly new as oxidative quenching by the electrolyte was never reported before in p-QDSSCs. This is also unusual with molecular sensitizers, where hole injection in NiO is the major deactivation process from the dye excited state.[20] Interestingly, the rates of both processes decrease as the diameter of PbS increases. The slower hole injection rate constant with bigger QDs can be understood as a consequence of the lower injection driving force (Table 2), while the decrease of the electrolyte reduction may originate from the fact that PbS is a p-type rather than a n-type semiconductor. Consequently in PbS, the electron extraction is less efficient than the hole, because the electron is trapped.

The rate of quenching of the PbS QDs by the quencher (cobalt, NiO or combination of both) is given by the additional rate of PL decay. We determine this by taking the natural logarithm of the ratio of the photoluminescence (PL) decay of QDs with quencher to the PL decay of QDs without quencher (i.e. on alumina substrate). This would give a horizontal line for no quenching (no electron or hole transfer) and line of a constant slope for a constant rate of electron or hole transfer. However, in Figure 3 we have a range of slopes indicating a strongly time dependent process. We determined these time dependent rates by differentiating the natural logarithm of the ratio according to equation 6:

$$k_{quench}(t) = -\frac{d}{dt}\left(log_e\left(\frac{PL\ of\ QD\ with\ acceptor}{PL\ of\ QD\ on\ alumina}\right)\right) \quad (6)$$

This quenching rate was determined by fitting the experimental data in Figure 3 (right panel) with three exponentials before differentiation. The resulting values of the quenching rates are plotted as a function of time in Figure 4 and clearly show that the quenching rate is strongly time dependent as

View Article Online
DOI: 10.1039/C7NR03698A

already observed before on NiO for other types of QDs,[32] but here we observe this behavior in a different nanocrystals of high importance for p-QDSSCs. In order to compare our results with previous studies, an average charge transfer rate was determined using the equation 7 below:

$$\langle k_{CT} \rangle = \frac{1}{\tau_1} \int_0^{\tau 1} k_{CT}(t)\, dt \qquad (7)$$

where τ_1 is the time for the fluorescence decay to fall to 1/e of its initial value. The obtained values of average charge transfer rates are given in Table 3. Caution should be taken when using this number as it is a gross simplification of the time dependent behaviour seen in Figure 4. The charge transfer efficiency (quantum yield) for each reaction was determined using the approach we reported previously (equation 8).[21]

$$\phi_{CT} = 1 - \frac{\int PL\ of\ QD\ with\ acceptor\ dt}{\int PL\ of\ QD\ on\ alumina} \qquad (8)$$

with $PL\ of\ QD\ with\ acceptor$ and $PL\ of\ QD\ on\ alumina$ are intensity decays of PbS QDs with quencher and without quencher i.e. on alumina substrate. The obtained values are given in Table 3.

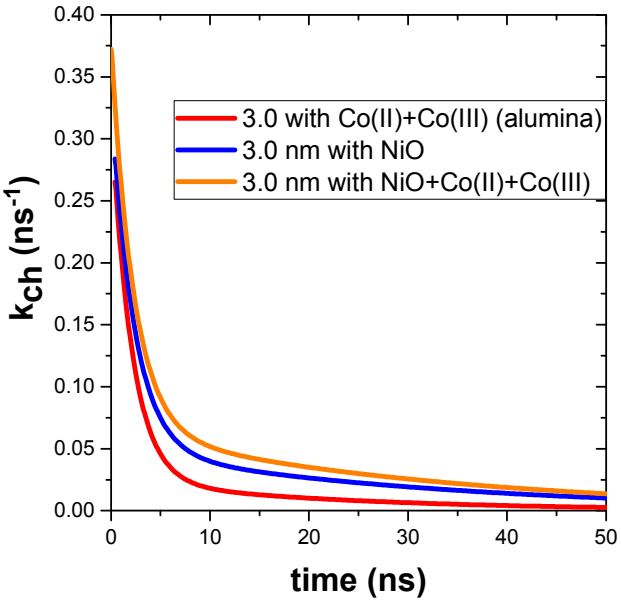

Figure 4. Charge transfer rate constants determined by differentiating the logarithm of PL ratios (right panel of Figure 3); blue line - on Al_2O_3 with solvent and with Co^{II} + Co^{III} complexes; red line - on NiO with solvent but without Co^{II} + Co^{III} complexes, orange line - on NiO with solvent and with Co^{II} + Co^{III} complexes.

View Article Online
DOI: 10.1039/C7NR03698A

Table 3. Rates constants and quantum yields of the hole injection and reductive quenching reactions from PbS exciton. $\langle k_{red}\ (s^{-1})\rangle$ is the rate of photoinduced electron transfer (reduction) to Co(II)+ Co(III) , $\langle k_{inj}\ (s^{-1})\rangle$ is hole injection rate constant to NiO and $\langle k_{inj+red}\ (s^{-1})\rangle$ is the combined rate constants of both electron and hole transfer to NiO and Co(II)+ Co(III).

Quencher		**3.0 nm**	**3.4 nm**	**4.0 nm**
none, $k_{PL}(s^{-1})$		1.5×10^7	2.4×10^7	2.8×10^7
Co(II)+Co(III)	$\langle k_{red}\ (s^{-1})\rangle$	1.3×10^8	5.5×10^7	1.4×10^7
	ϕ_{red} (%)	49	19	14
NiO (%)	$\langle k_{inj}\ (s^{-1})\rangle$	1.7×10^8	1.2×10^8	4.7×10^7
	ϕ_{inj} (%)	65	53	33
ratio $\langle k_{inj}\rangle/\langle k_{red}\rangle$		1.3	2.2	3.4
NiO+ Co(II)+Co(III)	$\langle k_{inj+red}\ (s^{-1})\rangle$	2.5×10^8	1.4×10^8	9.2×10^7
	$\phi_{inj+red}$ (%)	74	51	39

The rate constants for the hole injection reaction for the PbS QDs with diameter of 3.0, 3.4 and 4.0 nm are respectively 1.7×10^8 s^{-1}, 1.2×10^8 s^{-1} and 4.7×10^7 s^{-1} giving an injection quantum yield of 65%, 53% and 33 % respectively. Here, the injection rate constants measured with these PbS QDs are 10-50 times slower than those reported by Pullerits[6e] or Yeow[6d] with CdSe QD on NiO and 1000 times slower than from most molecular sensitizers.[1c, 19b, 20b-d, 22] This difference is most likely due the lower driving force with PbS (-0.2 eV vs -1 eV) and weaker electronic coupling than with molecular dyes, that are, usually, attached with a conjugated spacer to NiO. On the other hand, the rate constant for photoinduced electron transfer to Co(III) from the photoexcited PbS with diameter of 3.0, 3.4 and 4.0 nm are respectively 1.3×10^8 s^{-1}, 5.5×10^7 s^{-1} and 1.4×10^7 s^{-1} accounting for a (PbS)* + Co(III) → $PbS^{(+)}$ + Co(II) charge transfer quantum yield of 49%, 19% and 14% respectively. The ratio of hole injection relative to photoinduced electron transfer to Co(III) for PbS QDs with diameter of 3.0, 3.4 and 4.0 nm are 1.3, 2.2 and 3.4 respectively. These results indicate, firstly, that both reductive quenching (reaction 3 on Scheme 1), and oxidative quenching processes (reaction 4 on Scheme 1) occur in parallel during the cell operation and, secondly, that the rate of reduction of the Co(III) complex decreases more rapidly than the hole injection when the diameter of PbS increases. This is clearly reflected by the decreases by a factor of 3.6 of the hole injection rate constants while the reductive quenching is slowed down by almost a factor of 10 when the PbS diameter increases from 3.0 nm to 4.0 nm (Table

View Article Online
DOI: 10.1039/C7NR03698A

3). Interestingly, the quenching of PbS exciton by NiO or Co(III) is never quantitative even with the PbS with a diameter of 3.0 nm (Table 3). This result means that there is scope for greater progress if the traps in PbS are better passivated (enhancement of the intrinsic lifetime) or if the injection rate constant is increased (by using of a more suitable linker). It is important to note that all the processes, such as ligand exchange of OA on PbS with TBAI and all the fabrication steps of solar cells, were accomplished under ambient atmosphere, since a glove box was never used. As a consequence, the concentration of traps states on PbS is certainly larger than that can be achieved with optimized procedures and conducted under inert atmosphere.[23] Optimization can be also envisioned with the use of another redox mediator with faster regeneration rate constant than cobalt polypyridine complexes, because they are known to be slow acceptors owing to spin change and non-adiabatic electron transfer.[20a, 24]

Photovoltaic performances in p-DSSCs

The PbS quantum dots were immobilized on mesoporous NiO with the traditional linker assisted methodology, which was previously developed as it proved to be particularly suited for this purpose in p-QDSSCs.[10] It is important to mention that NiO nanoparticles were deposited by screen printing on a thin dense layer of NiO and not directly on FTO surface. Indeed, we observed that the direct contact of PbS on FTO glass leads to the appearance of an anodic photocurrent (probably due to electron injection in FTO substrate from PbS exciton), which counterbalances the searched cathodic photocurrent (hole injection into NiO). This result agrees with previous reports.[25] Moreover, it is known that the presence of a NiO dense layer improves the adhesion of NiO nanoparticles to the transparent electrode and reduces the interfacial charge recombination with the electrolyte.[1g, 26] Finally, the sintered NiO films were soaked into an ethanolic solution of nickel acetate to diminish the surface nickel oxide recombination sites and to improve the NiO nanoparticles necking.[27] The redox couple used in this study was the cobalt complexes: *tris*(4,4'-di*tert*-butyl-2,2'-bipyridine)cobalt(III/II) (structure given in Figure S5), because it is fully compatible and not corrosive with the PbS quantum dots that are reputed to be corroded with iodine and polysulfide based electrolytes.[28] The solar cells were all fabricated with the PbS quantum dots treated with TBAI, since the initial oleic acid capped nanocrystals give much lower photovoltaic performances as we have already reported before.[10] This is most certainly due to the shorter lifetime of the exciton, which decreases the injection quantum yield. The metrics of the solar cells are collected in Table 3, the photoaction spectra (Incident photon-to-current efficiency (IPCE) as a function of incident wavelength) are shown in Figure 5 and the current/voltage characteristics are given in Figure S6. The values given in Table 4 correspond to the average of the results recorded on six independent solar cells.

View Article Online
DOI: 10.1039/C7NR03698A

Table 4. Photovoltaic performances of NiO-based p-QDSSCs recorded under simulated solar light AM1.5 (100 mW/cm^2) as a function of the PbS diameter.

d (nm)	V_{OC} (mV)	J_{SC} (mA.cm^{-2})	ff (%)	PCE (%)
2.8	185 (±15)	4.2 (±0.20)	33 (±1)	0.25 (±0.02)
2.9	180 (±10)	4.5 (±0.15)	32 (±2)	0.26 (±0.01)
3.0	175 (±10)	5.1 (±0.20)	33 (±1)	0.29 (±0.01)
3.2	160 (±15)	3.7 (±0.12)	30 (±1)	0.17 (±0.05)
3.4	150 (±20)	3.1 (±0.10)	29 (±1)	0.13 (±0.07)
4.0	90 (±30)	2.5 (±0.13)	27 (±2)	0.03 (0.01)

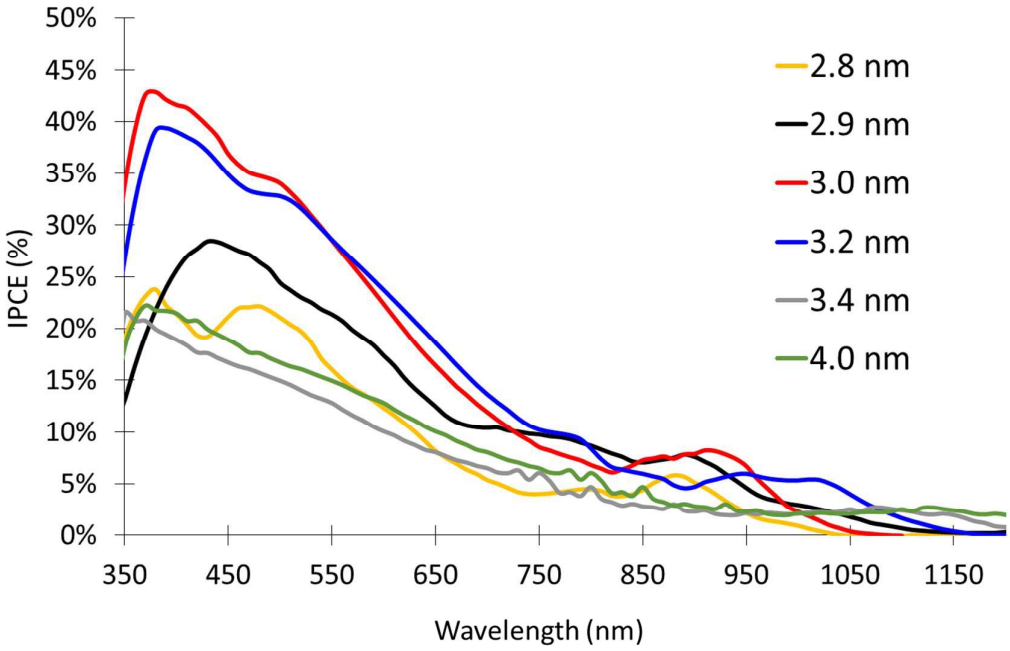

Figure 5. Photoaction spectra of the NiO based p-DSSC sensitized with PbS QDs of different sizes.

Inspection of the IPCE spectra shows that as the bandgap of the QD decreases, the IPCE values, particularly on the exciton band, increase and shift to the lower energy part of the solar spectrum, but when the size goes above 3 nm, the maximum IPCE values decrease, reflecting a diminution of the

View Article Online
DOI: 10.1039/C7NR03698A

injection efficiency. In the IPCE spectra, we can also notice that the high energy maximum absorption peak of the large quantum dots (3.4 and 4.0 nm) is not any more discernible. This certainly due to a combination of factors, that are the lower injection quantum yield of the large size QDs (owing to low injection driving force), the significant absorbance of NiO film and possibly light scattering. Moreover, the absorption of the redox mediator is too weak to cause the observed change (see Figure S7).

Clearly, the photovoltaic performance is dependent on the size of the nanocrystal with the maximum performance measured for PbS quantum dots of 3.0 nm diameter. First, the Voc steadily decreases as a function of the PbS size. This is a quite general behavior already observed on TiO_2 based DSSCs since low bandgap QDs usually display lower Voc than larger ones.[29] On the other hand, the Jsc increases for sizes from 2.8 to 3.0 nm and then decreases for larger sizes (Table 4). The photocurrent density is proportional to the light harvesting efficiency (LHE), the injection quantum yield (ϕ_{inj}) and the charge collection efficiency (η_{charge}):

$$Jsc \alpha LHE \times \phi_{inj} \times \eta_{charge} \qquad (9)$$

The absorption spectra in Figure 2 indicate that the LHE increases with the size of PbS nanocrystal because the band is extended towards the low energy region with an increase in absorption coefficient (Table 1); therefore the growth of Jsc from 2.8 nm to 3.0 nm is certainly the consequence of higher LHE. This is corroborated by the IPCE spectra, which span to longer wavelength and reach higher values as the diameter of PbS increases from 2.8 to 3.0 nm (Figure 5). The drop of Jsc for larger diameter than 3.0 nm indicates that lower charge regeneration and hole injection efficiencies counterbalance the higher LHE (see below). Therefore, there is a trade-off effects of the light-harvesting and the hole injection efficiency that lead to the highest Jsc for PbS nanocrystal of 3.0 nm. The charge collection efficiency is controlled by the regeneration reaction of the reduced PbS by the redox couple. The rate constant of the reduction of Co(III) from the exciton is more size dependent than the hole injection reaction (Table 2), we can therefore conclude that this will be most probably the case for the electron shift from the reduced PbS to the Co(III) complex in the electrolyte. As a result, the efficiency of the electron shift from reduced PbS to Co(III) (reaction 4 on Scheme 1) may control the Jsc, since this process slows down as the diameter of PbS increases. Moreover, this process is in competition with the charge recombination (CR) from the injected hole in NiO and the electron residing in the conduction band of PbS (reaction 5 in Scheme 1). The slower rate of PbS regeneration as the size of PbS increases will naturally decrease the charge collection efficiency, because the CR pathway is very acute in p-DSSCs owing to the presence of an intragap states and the location of recombination centers at the surface of the NiO.[30] In addition, the oxidative quenching of PbS by Co(III) diminishes more steeply than hole injection on NiO, therefore we can assume that regeneration of the oxidized PbS controls the photocurrent density. In other words, improving electron transfer

View Article Online
DOI: 10.1039/C7NR03698A

from PbS to the redox mediator could be a favorable strategy to enhance the photovoltaic performance of these p-QDSSCs. Finally, the efficiency of the hole injection quantum yield also drops with the size of PbS, because of the reduced injection driving force (Table 2); therefore the slower rate of this reaction in combination with the shorter intrinsic lifetime of large PbS both lead to a diminution of the injection quantum yield and necessarily to the Jsc (Table 4). Overall, the decrease of the photovoltaic performance of the solar cells when the size of the PbS nanocrystal is raised above 3 nm can be understood as a decrease of both of the regeneration and the hole injection efficiencies. Oxidative quenching (reaction 4) cannot account on its own for the total photocurrent production, because the reductive quenching quantum yield is lower than the maximum value of IPCE with PbS of diameter 3.4 and 4 nm (IPCE at 400 nm reaches 22% and 20% for PbS diameter of 3.4 and 4 nm respectively, while ϕ_{red} is only 19 and 14%). As a consequence, reductive quenching of PbS* by NiO (reaction 3), that is the decay of PbS exciton first by hole injection in NiO, is necessarily an operative pathway to produce electricity. On the other hand, the direct reduction of the electrolyte from the photoexcited PbS is certainly also an effective process during the cell operation because CR between the reduced redox mediator (Co(II) species) and hole in PbS is most certainly slower than hole injection from PbS^{+}(bimolecular process with two species positively charged), since hole injection from PbS* occurs in a few nanoseconds. These results have important implications for the future design of QD sensitized cathodes, because firstly it indicates that direct reductive quenching of the photoexcited QD (by a redox mediator for p-DSSC or by a reduction catalyst for solar fuel production in DSPECs) can be a favorable pathway to attain large photocurrent densities. Additionally, this work demonstrates that efficient hole injection in NiO with low bandgap QDs can occur even with a low driving force. This result is in sharp contrast with what is usually accepted with molecular sensitizers in p-DSSCs, for which a minimum of 0.6 eV driving is necessary to ensure efficient hole injection in NiO.[31]

Conclusion

In this work, we optimized the energy band alignment, rates of charge transfer at the interface and resulting photovoltaic performance of QDSSCs by controlling the size of the PbS nanocrystal. For this we have synthesized a series of PbS QDs with different diameters and investigated their ability to act as sensitizers in NiO based solar cells. Towards this goal, the quantum dots were fully characterized by absorption and emission spectra and by electrochemistry. Additionally, time-resolved emission spectroscopy of the PbS luminescence measured on different surface (Al_2O_3 and NiO) and in different environments (presence or absence of the redox shuttle) enabled to determination of the rate constants for the hole injection and for the oxidative quenching by the electrolyte from the photoexcited PbS. The photovoltaic performance of the nanocrystals was also determined in NiO based p-QDSSCs with a cobalt complex as redox mediator. Highly performing stand-alone NiO based photocathode for solar cells (power conversion efficiency above 10%) may be limited by the shallow valence band potential

View Article Online
DOI: 10.1039/C7NR03698A

of NiO, that will make it difficult to reach high open circuit potential (Voc) unless very negative redox potential are used.[32] This study demonstrates that the optimal size of PbS to sensitize mesoporous NiO films is 3.0 nm. The photophysical study rationalizes the influence of the size of PbS quantum dot on the photovoltaic performances of PbS nanocrystals in p-QDSSCs. It first demonstrates that hole injection in NiO from the photoexcited QD is an efficient process even with low injection driving force. Second, the direct electrolyte reduction by the QD is a competing process of the hole injection, that occurs in parallel with a significant quantum yield. However, the reductive quenching of PbS by the reduced form of the redox mediator (here Co(II)) can be favorable to produce electricity, because the charge recombination from the reduced QD with the redox mediator is most probably slower than the charge recombination with the hole in NiO. These results suggest that efficient photocathodes can be prepared with low bandgap nanocrystals and that initial hole injection from the photoexcited QD is not necessarily the only process to generate electricity in QD sensitized photocathode. Another direct consequence of this finding is the probable important impact of the linker used to connect the QD to the NiO, because depending of its length and its electronic properties it will most certainly impact the ratio of the hole injection and electron transfer processes (k_{inj}/k_{red}) and consequently the photocurrent density produced by the system. In addition, better passivation of traps in PbS QDS with improved strategies (new procedures, core/shell structure and preparation of the samples under inert atmosphere) should lead to even higher photovoltaic performance of PbS QDs. Finally, new redox mediators with lower reorganization energy than polypyridine cobalt complexes might be better suited to maximize the electron transfer reaction from PbS to the electrolyte. These results represent new and critical information to consider for the future design of QD sensitized photocathodes for photovoltaic and photocatalysis.

Acknowledgements

ANR is gratefully acknowledged for the financial support of these researches through the QuePhelec project (n° ANR-13-BS10-0011-01). Région des Pays de la Loire and Nantes University for the project LUMOMAT are also acknowledged. We acknowledge support from the European Research Council (grant number 321305) and the EPSRC (grant number EP/L017008/1). IDWS is a Royal Society Wolfson Research Merit award holder.

Supporting information available: Preparation of the PbS QDs, fabrication of the p-QDSSCs, absorption and emission spectra of the PbS-TBAI QDs, photophysical study of 3.4 nm and 4.0 nm PbS-TBAI QDs and PL decays of 3.0 nm, 3.4 nm and 4.0 nm PbS-TBAI QDs is presented

View Article Online
DOI: 10.1039/C7NR03698A

in supporting information. The research data supporting this publication can be accessed at http://dx.doi.org/10.17630/ddaebfb9-e127-43cb-9048-966a572b50ac.

References

1. (a) S. Powar, R. Bhargava, T. Daeneke, G. Götz, P. Bäuerle, T. Geiger, S. Kuster, F. A. Nüesch, L. Spiccia and U. Bach, *Electrochimica Acta*, 2015, **182**, 458-463; (b) D. Xiong and W. Chen, *Front. Optoelectron.*, 2012, **5**, 371-389; (c) A. Nattestad, A. J. Mozer, M. K. R. Fischer, Y. B. Cheng, A. Mishra, P. Baeuerle and U. Bach, *Nat. Mater.*, 2010, **9**, 31-35; (d) A. Nakasa, H. Usami, S. Sumikura, S. Hasegawa, T. Koyama and E. Suzuki, *Chem. Lett.*, 2005, **34**, 500-501; (e) J. He, H. Lindström, A. Hagfeldt and S. E. Lindquist, *Sol. Energy Mater. Sol. Cells* 2000, **62**, 265-273; (f) F. Odobel, Y. Pellegrin, F. B. Anne and D. Jacquemin, in *High-Efficiency Solar Cells: Physics, Materials, and Devices*, eds. X. Wang and Z. M. Wang, Springer International Publishing, Cham, 2014, pp. 215-246; (g) E. A. Gibson, A. L. Smeigh, L. L. Pleux, J. Fortage, G. Boschloo, E. Blart, Y. Pellegrin, F. Odobel, A. Hagfeldt and L. Hammarström, *Angew. Chem. Int. Ed.*, 2009, **48**, 4402-4405; (h) C. J. Wood, G. H. Summers and E. A. Gibson, *Chem. Commun.*, 2015, **51**, 3915-3918; (i) Y. H. Lee, J. Y. Park, S. Thogiti, R. Cheruku and J. H. Kim, *Electron. Mater. Lett.*, 2016, **12**, 524-529.
2. (a) F. Li, K. Fan, B. Xu, E. Gabrielsson, Q. Daniel, L. Li and L. Sun, *J. Am. Chem. Soc.*, 2015, **137**, 9153-9159; (b) K. A. Click, D. R. Beauchamp, Z. Huang, W. Chen and Y. Wu, *J. Am. Chem. Soc.*, 2016, **138**, 1174-1179; (c) L. Tong, A. Iwase, A. Nattestad, U. Bach, M. Weidelener, G. Gotz, A. Mishra, P. Bäuerle, R. Amal, G. G. Wallace and A. J. Mozer, *Energy Environ. Sci.*, 2012, **5**, 9472-9475; (d) N. Kaeffer, J. Massin, C. Lebrun, O. Renault, M. Chavarot-Kerlidou and V. Artero, *J. Am. Chem. Soc.*, 2016, **138**, 12308-12311.
3. G. Sahara, H. Kumagai, K. Maeda, N. Kaeffer, V. Artero, M. Higashi, R. Abe and O. Ishitani, *J. Am. Chem. Soc.*, 2016, **138**, 14152-14158.
4. (a) K. Zhao, Z. Pan, I. Mora-Seró, E. Cánovas, H. Wang, Y. Song, X. Gong, J. Wang, M. Bonn, J. Bisquert and X. Zhong, *J. Am. Chem. Soc.*, 2015, **137**, 5602-5609; (b) J. Du, Z. Du, J.-S. Hu, Z. Pan, Q. Shen, J. Sun, D. Long, H. Dong, L. Sun, X. Zhong and L.-J. Wan, *J. Am. Chem. Soc.*, 2016, **138**, 4201-4209; (c) P. V. Kamat, *J. Phys. Chem. Lett.*, 2013, **4**, 908-918; (d) I. Hod and A. Zaban, *Langmuir*, 2014, **30**, 7264-7273; (e) P. V. Kamat, K. Tvrdy, D. R. Baker and J. G. Radich, *Chem. Rev.*, 2010, **110**, 6664-6688; (f) G. H. Carey, A. L. Abdelhady, Z. Ning, S. M. Thon, O. M. Bakr and E. H. Sargent, *Chem. Rev.*, 2015, **115**, 12732-12763.
5. (a) I. Barcelo, E. Guillen, T. Lana-Villarreal and R. Gomez, *J. Phys. Chem. C*, 2013, **117**, 22509-22517; (b) Y. Na, B. Hu, Q.-L. Yang, J. Liu, L. Zhou, R.-Q. Fan and Y.-L. Yang, *Chin. Chem. Lett.*, 2015, **26**, 141-144; (c) F. Safari-Alamuti, J. R. Jennings, M. A. Hossain, L. Y. L. Yung and Q. Wang, *Phys. Chem. Chem. Phys.*, 2013, **15**, 4767-4774.
6. (a) P. Meng, M. Wang, Y. Yang, S. Zhang and L. Sun, *J. Mater. Chem. A*, 2015, **3**, 18852-18859; (b) M.-A. Park, S.-Y. Lee, J.-H. Kim, S.-H. Kang, H. Kim, C.-J. Choi and K.-S. Ahn, *Mol. Cryst. Liq. Cryst.*, 2014, **598**, 154-162; (c) M.-A. Park, S.-Y. Lee, J.-H. Kim, S.-H. Kang, H. Kim, C.-J. Choi and K.-S. Ahn, *Phys. Status Solidi A*, 2014, **211**, 1868-1872; (d) X. Wu and E. K. L. Yeow, *Chem. Commun.*, 2010, **46**, 4390-4392; (e) K. Zheng, K. Žídek, M. Abdellah, W. Zhang, P. Chábera, N. Lenngren, A. Yartsev and T. Pullerits, *J. Phys. Chem. C*, 2014, **118**, 18462-18471.
7. J. H. Rhee, Y. H. Lee, P. Bera and S. I. Seok, *Chem. Phys. Lett.*, 2009, **477**, 345-348.
8. C. Zhao, X. Zou and S. He, *J. Nanomater.*, 2014, 372381/372381-372381/372386, 372386 pp.
9. (a) T. J. Macdonald, Y. J. Mange, M. R. Dewi, H. U. Islam, I. P. Parkin, W. M. Skinner and T. Nann, *J. Mater. Chem.A*, 2015, **3**, 13324-13331; (b) J. Park, M. T. Sajjad, P.-H. Jouneau, A. Ruseckas, J. Faure-Vincent, I. D. W. Samuel, P. Reiss and D. Aldakov, *J. Mater. Chem. A*, 2016, **4**, 827-837.
10. M. Raissi, Y. Pellegrin, S. Jobic, M. Boujtita and F. Odobel, *Sci. Rep.*, 2016, **6**, doi: 10.1038/srep24908.

View Article Online
DOI: 10.1039/C7NR03698A

11. (a) H. B. Yang, J. Miao, S.-F. Hung, F. Huo, H. M. Chen and B. Liu, *ACS Nano*, 2014, **8**, 10403-10413; (b) B. Liu, X.-B. Li, Y.-J. Gao, Z.-J. Li, Q.-Y. Meng, C.-H. Tung and L.-Z. Wu, *Energy Environ. Sci.*, 2015, **8**, 1443-1449; (c) T. P. A. Ruberu, Y. Dong, A. Das and R. Eisenberg, *ACS Catal.*, 2015, 2255-2259; (d) Y. Dong, R. Wu, P. Jiang, G. Wang, Y. Chen, X. Wu and C. Zhang, *ACS Sustain. Chem. Eng.*, 2015, **3**, 2429-2434.
12. (a) H. Wang, T. Kubo, J. Nakazaki, T. Kinoshita and H. Segawa, *J. Phys. Chem. Lett.*, 2013, **4**, 2455-2460; (b) S. Jiao, J. Wang, Q. Shen, Y. Li and X. Zhong, *J. Mater. Chem. A*, 2016, **4**, 7214-7221; (c) G.-H. Kim, F. P. García de Arquer, Y. J. Yoon, X. Lan, M. Liu, O. Voznyy, Z. Yang, F. Fan, A. H. Ip, P. Kanjanaboos, S. Hoogland, J. Y. Kim and E. H. Sargent, *Nano Lett.*, 2015, **15**, 7691-7696.
13. (a) M. A. Hines and G. D. Scholes, *Adv. Mater.*, 2003, **15**, 1844-1849; (b) J. Zhang, R. W. Crisp, J. Gao, D. M. Kroupa, M. C. Beard and J. M. Luther, *J. Phys. Chem. Lett.*, 2015, **6**, 1830-1833.
14. (a) J. Tang, K. W. Kemp, S. Hoogland, K. S. Jeong, H. Liu, L. Levina, M. Furukawa, X. Wang, R. Debnath, D. Cha, K. W. Chou, A. Fischer, A. Amassian, J. B. Asbury and E. H. Sargent, *Nat. Mater.*, 2011, **10**, 765-771; (b) A. H. Ip, S. M. Thon, S. Hoogland, O. Voznyy, D. Zhitomirsky, R. Debnath, L. Levina, L. R. Rollny, G. H. Carey, A. Fischer, K. W. Kemp, I. J. Kramer, Z. Ning, A. J. Labelle, K. W. Chou, A. Amassian and E. H. Sargent, *Nat. Nano*, 2012, **7**, 577-582.
15. M. Yuan, M. Liu and E. H. Sargent, *Nature Energy*, 2016, **1**, 16016.
16. I. Moreels, K. Lambert, D. Smeets, D. De Muynck, T. Nollet, J. C. Martins, F. Vanhaecke, A. Vantomme, C. Delerue, G. Allan and Z. Hens, *ACS Nano*, 2009, **3**, 3023-3030.
17. L. Cademartiri, E. Montanari, G. Calestani, A. Migliori, A. Guagliardi and G. A. Ozin, *J. Am. Chem. Soc.*, 2006, **128**, 10337-10346.
18. (a) B.-R. Hyun, Y.-W. Zhong, A. C. Bartnik, L. Sun, H. D. Abruña, F. W. Wise, J. D. Goodreau, J. R. Matthews, T. M. Leslie and N. F. Borrelli, *ACS Nano*, 2008, **2**, 2206-2212; (b) A. S. Cuharuc, L. L. Kulyuk, R. I. Lascova, A. A. Mitioglu and A. I. Dikusar, *Surface Engineering Appl. Electrochem.*, 2012, **48**, 193-211.
19. (a) F. Odobel and Y. Pellegrin, *J. Phys. Chem. Lett.*, 2013, **4**, 2551-2564; (b) F. Odobel, Y. Pellegrin, E. A. Gibson, A. Hagfeldt, A. L. Smeigh and L. Hammarström, *Coord. Chem. Rev.*, 2012, **256**, 2414-2423.
20. (a) E. A. Gibson, A. L. Smeigh, L. Le Pleux, L. Hammarström, F. Odobel, G. Boschloo and A. Hagfeldt, *J. Phys. Chem. C* 2011, **115**, 9772-9779; (b) A. Morandeira, G. Boschloo, A. Hagfeldt and L. Hammarström, *J. Phys. Chem. B*, 2005, **109**, 19403-19410; (c) A. Morandeira, G. Boschloo, A. Hagfeldt and L. Hammarström, *J. Phys. Chem. C*, 2008, **112**, 9530-9537; (d) L. Le Pleux, A. L. Smeigh, E. Gibson, Y. Pellegrin, E. Blart, G. Boschloo, A. Hagfeldt, L. Hammarström and F. Odobel, *Energy Environ. Sci.*, 2011, **4**, 2075-2084.
21. D. Aldakov, M. T. Sajjad, V. Ivanova, A. K. Bansal, J. Park, P. Reiss and I. D. Samuel, *Journal of Materials Chemistry A*, 2015, **3**, 19050-19060.
22. (a) L. Zhang, L. Favereau, Y. Farre, E. Mijangos, Y. Pellegrin, E. Blart, F. Odobel and L. Hammarstrom, *Phys. Chem. Chem. Phys.*, 2016, **18**, 18515-18527; (b) P. Qin, J. Wiberg, E. A. Gibson, M. Linder, L. Li, T. Brinck, A. Hagfeldt, B. Albinsson and L. Sun, *J. Phys. Chem. C* 2010, **114**, 4738-4748.
23. X. Lan, O. Voznyy, F. P. García de Arquer, M. Liu, J. Xu, A. H. Proppe, G. Walters, F. Fan, H. Tan, M. Liu, Z. Yang, S. Hoogland and E. H. Sargent, *Nano Letters*, 2016, **16**, 4630-4634.
24. (a) M. J. Weaver and E. L. Yee, *Inorg. Chem.*, 1980, **19**, 1936-1945; (b) Y. Xie and T. W. Hamann, *J. Phys. Chem. Lett.*, 2013, **4**, 328-332.
25. (a) H. Wang, X. Zeng, Z. Huang, W. Zhang, X. Qiao, B. Hu, X. Zou, M. Wang, Y.-B. Cheng and W. Chen, *ACS Appl. Mater. Interfaces*, 2014, **6**, 12609-12617; (b) R. Narayanan, B. N. Reddy and M. Deepa, *J. Phys. Chem. C*, 2012, **116**, 7189-7199.
26. P. Ho, L. Q. Bao, K.-S. Ahn, R. Cheruku and J. H. Kim, *Synthetic Metals*, 2016, **217**, 314-321.
27. Q. Liu, L. Wei, S. Yuan, X. Ren, Y. Zhao, Z. Wang, M. Zhang, L. Shi and D. Li, *J. Mater. Sci.*, 2015, **50**, 6668-6676.
28. S. D. Sung, I. Lim, P. Kang, C. Lee and W. I. Lee, *Chem. Commun.*, 2013, **49**, 6054-6056.

View Article Online
DOI: 10.1039/C7NR03698A

29. (a) H. Zhang, K. Cheng, Y. M. Hou, Z. Fang, Z. X. Pan, W. J. Wu, J. L. Hua and X. H. Zhong, *Chem. Commun.*, 2012, **48**, 11235-11237; (b) H. J. Yun, T. Paik, B. Diroll, M. E. Edley, J. B. Baxter and C. B. Murray, *ACS Appl. Mater. Interfaces*, 2016, **8**, 14692-14700.
30. (a) A. L. Smeigh, L. L. Pleux, J. Fortage, Y. Pellegrin, E. Blart, F. Odobel and L. Hammarström, *Chem. Commun.*, 2012, **48,** , 678-680; (b) L. D'Amario, L. J. Antila, B. Pettersson Rimgard, G. Boschloo and L. Hammarström, *J. Phys. Chem. Lett.*, 2015, **6**, 779-783; (c) L. D'Amario, R. Jiang, U. B. Cappel, E. A. Gibson, G. Boschloo, H. Rensmo, L. Sun, L. Hammarström and H. Tian, *ACS Appl. Mater. Interfaces*, 2017; (d) L. Favereau, Y. Pellegrin, L. Hirsch, A. Renaud, A. Planchat, E. Blart, G. Louarn, L. Cario, S. Jobic, M. Boujtita and F. Odobel, *Adv. Energy Mater.*, 2017, **7**, doi: 10.1002/aenm.201601776.
31. T. Daeneke, Z. Yu, G. P. Lee, D. Fu, N. W. Duffy, S. Makuta, Y. Tachibana, L. Spiccia, A. Mishra, P. Bäuerle and U. Bach, *Adv. Energy Mater.*, 2015, **5**, 10.1002/aenm.201401387.
32. (a) S. Powar, T. Daeneke, M. T. Ma, D. Fu, N. W. Duffy, G. Götz, M. Weidelener, A. Mishra, P. Bäuerle, L. Spiccia and U. Bach, *Angew. Chem. Int. Ed.*, 2013, **52**, 602-605; (b) I. R. Perera, T. Daeneke, S. Makuta, Z. Yu, Y. Tachibana, A. Mishra, P. Bäuerle, C. A. Ohlin, U. Bach and L. Spiccia, *Angew. Chem. Int. Ed.*, 2015, **54**, 3758-3762.